Nuclear Inst. and Methods in Physics Research, A 1054 (2023) 168392

Contents lists available at ScienceDirect

Nuclear Inst. and Methods in Physics Research, A

journal homepage: www.elsevier.com/locate/nima

Review

Position-resolved timing characterisation tests of hexagonal and trench 3D silicon detectors

Matthew Addison [a,*], Cinzia Da Via [a], Adriano Lai [b], Gian-Franco Dalla Betta [c], Michela Garau [b], Andrea Lampis [b], Mauro Aresti [b], Alessandro Cardini [b], Gian-Matteo Cossu [b], Angelo Loi [b]

[a] Physics and Astronomy, The University of Manchester, UK
[b] INFN, Cagliari, Italy
[c] The University of Trento, Italy

ARTICLE INFO

Keywords:
3D silicon
Timing characterisation

ABSTRACT

Position-resolved timing characterisation tests were performed on individual pixels of hexagonal and trench 3D silicon sensors. An IR laser was used to deposit energy equivalent to 1 MIP with a 1 μm spatial resolution onto each sensor, which were attached to custom-designed fast read-out electronics chips. Time of Arrival (ToA) values obtained were (544 ± 29.8) ps for the hexagonal geometry, and (515 ± 8.2) ps for the trench geometry.

Contents

1. Introduction 1
2. Pixel geometries 1
3. Front-end electronics 1
4. Experimental method 2
5. Data analysis and results 2
6. Conclusion 3
Declaration of competing interest 3
Acknowledgements 3
References 3

1. Introduction

Upgrades to the LHC will see integrated beam luminosity increase by up to a factor of 7, requiring the development of radiation-hard, fast-timing detectors. In order to perform track and vertex reconstruction after the upgrades, some experiments of the LHC have estimated that timing resolutions of 10–50 ps are required for their vertex detectors [1]. 3D silicon sensors are being developed that are able to withstand the projected radiation levels of HL-LHC and keep within the estimated required timing resolution [2,3]. 3D sensors hold a major advantage over their planar counterparts as inter-electrode distance is decoupled from and can be made significantly shorter than the substrate thickness, as illustrated in Fig. 1.

This results in increased charge collection efficiency, reduced charge sharing, lower depletion voltages and the ability to include an active edge in the sensor design [4].

2. Pixel geometries

Microscope images of hexagonal and trench pixel sensors are shown in Figs. 2a and 2b, whilst illustrations of the geometries and dimensions of these pixels are shown in Figs. 2c and 2d.

In both sensors, aluminium contacts allow signal read-out from the central electrode but also block the IR laser, meaning that part of each sensor geometry is invisible to a laser scan.

3. Front-end electronics

Developed by the TimeSPOT collaboration, the front-end electronics is based on a single-channel, two-stage amplification scheme that acts as a trans-impedance amplifier. AC-coupled Si-Ge bipolar transistors are used for applications that are low in noise and high in bandwidth. Current amplifiers that have been designed for fast signals are used, and are based on a monolithic wide-band amplifier [5].

* Corresponding author.
E-mail address: matthew.addison@manchester.ac.uk (M. Addison).

https://doi.org/10.1016/j.nima.2023.168392
Received 28 July 2022; Received in revised form 6 April 2023; Accepted 4 May 2023
Available online 10 June 2023

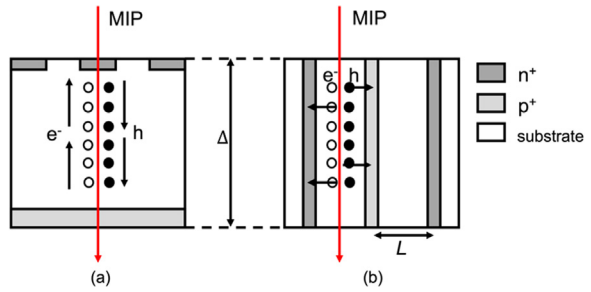

Fig. 1. Illustration of the differences between inter-electrode distance and therefore the distance travelled by ionised electrons and holes in (a) planar sensors and (b) 3D sensors.

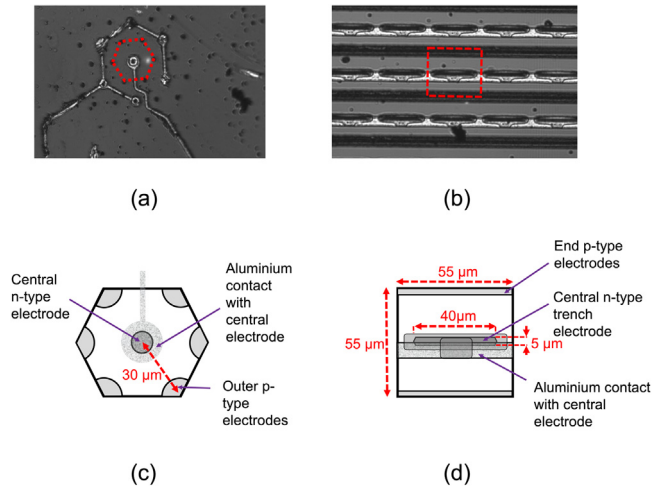

Fig. 2. Images of individual pixels of the (a) hexagonal and (b) trench electrode silicon sensors being characterised. Schematic drawings of single pixels of the (c) hexagonal and (d) trench sensor geometries. Both pixels feature an active thickness of 150 μm, a central n-type read-out electrode and outer p-type electrodes to which the external −50 V bias is applied.

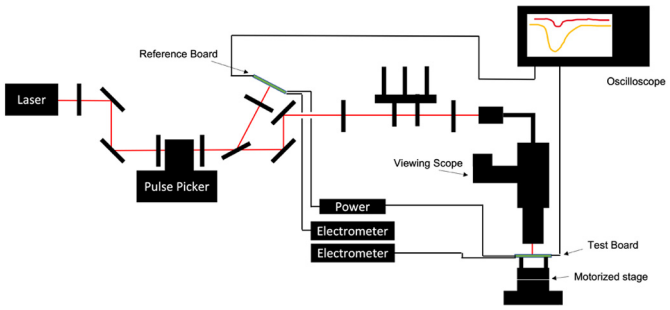

Fig. 3. Schematic drawing of the lay-out of the equipment used to perform the time characterisation tests. The pulse picker was not used for this data acquisition.

4. Experimental method

A schematic drawing of the set-up is shown in Fig. 3.

An IR laser with a wavelength of 1030 nm was passed through a series of lenses and mirrors [6]. Using a beam-splitter, part of the beam split off to a reference sensor and deposited energy roughly equivalent to 10 MIPs. The remainder of the beam deposited energy equivalent to 1 MIP on the test sensor. A silicon test structure was used for the reference sensor, with a 0.03 mm^2 active area and 907 fs timing accuracy [1]. Sensors were attached to PCB boards, allowing a reverse bias to be applied, with a −100 V bias used for the reference board in all tests. Each board was connected to an oscilloscope, which displayed the output voltage signal for each board as a function of time. The oscilloscope used had 4 channels, a sampling rate of 20 $GSas^{-1}$ and an analog bandwidth of 8 GHz.

In turn, each of the sensor test geometries were connected to the set-up, with a −50 V reverse bias applied to each. This reverse bias value was chosen as it ensured full depletion and charge carrier velocity saturation, whilst keeping the leakage current at an appropriately low value. The laser spot of the set-up was aimed onto the sensor pixel being characterised. Using LabView, a scan of each pixel was performed, using 1 μm increments in x and y. The output settings of the oscilloscope were altered such that for each laser position, 1000 waveforms of both the reference and test signal were outputted. This meant that the effects of electronic jitter were heavily suppressed in the results, and the timing resolution determined is a consequence of the non-uniformity of the weighting field in each pixel.

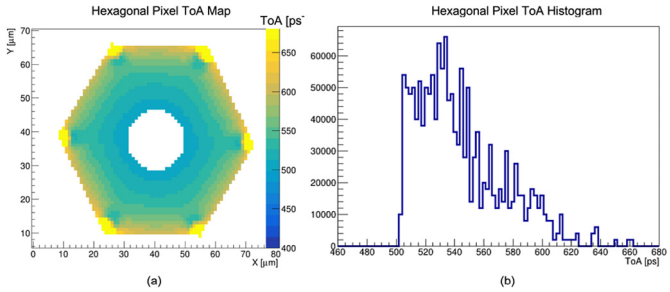

Fig. 4. (a) ToA map and (b) ToA histograms for the hexagonal pixel sensor geometry. Non-uniformities of the weighting field within the active region of the hexagonal pixel gives rise to a broader ToA histogram.

5. Data analysis and results

Each outputted waveform contained signal amplitude information as a function of time. A 35% constant fraction discriminator was applied to each waveform to assign a time-stamp to each signal. Time of arrival (ToA) of each test signal was determined by taking the time stamp of a given test signal and subtracting the time stamp of its corresponding reference signal.

To remove as many regions covered by aluminium as possible, geometric cuts were performed on both pixels to isolate the half of the pixel with less covering aluminium. These isolated halves were then duplicated, rotated and translated in order to obtain a fuller pixel image for both types of sensor. In both pixels, the mean ToA for each position of the scan was calculated, and the overall ToA value was determined from these position-specific mean ToA values.

The ToA map and histogram for the hexagonal pixel geometry are shown respectively in Figs. 4a and 4b.

The ToA of the hexagonal pixel was (544 ± 29.8) ps. Regions between two adjacent outer electrodes have a lower field and hence electron–hole pairs must diffuse to higher field regions before they can drift and be detected [7]. By considering the weighting field of the hexagonal pixel (as shown in Fig. 5a), it is noticed that the high field region of the pixel is covered by the aluminium contacts, meaning that the fastest regions of the sensor are not included in these results.

A pronounced tail is observed in the ToA histogram as a consequence of slow regions in the pixel periphery, suggesting the potential presence of inefficiencies in charge collection when fast electronics are used.

The ToA map and histogram for the trench pixel geometry are shown respectively in Figs. 6a and 6b.

The ToA of the trench pixel was (515 ± 8.2) ps. There is minimal spread in ToA values over the active region of the sensor due to the high uniformity of the weighting field within this region. The lowest

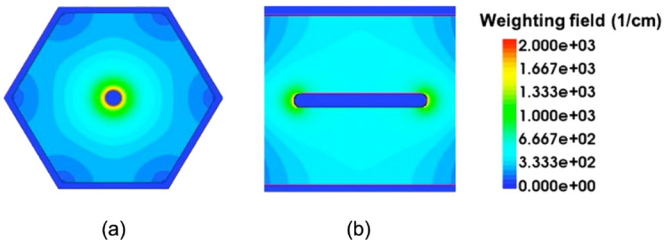

Fig. 5. TCAD simulations of the weighting field of (a) hexagonal and (b) trench 3D silicon pixel sensors [8].

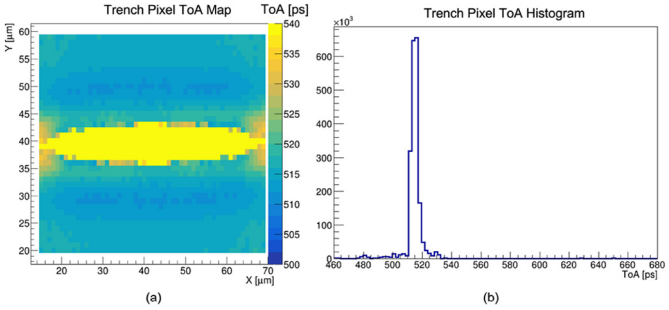

Fig. 6. (a) ToA map and (b) ToA histogram for the trench pixel sensor geometry. Owing to the highly uniform weighting field within the active region of the trench pixel, the ToA histogram is well-defined.

field regions of this sensor are covered by the aluminium contacts and so do not form a part of these results. By observing the weighting field of the trench pixel as shown in Fig. 5b, this can be confirmed.

6. Conclusion

The hexagonal sensor geometry exhibits an excellent timing performance, with a timing resolution of 29.8 ps, falling within the timing requirement of 50 ps due to be imposed by HL-LHC. The trench sensor geometry has even better timing performance, with a timing resolution of 8.2 ps. The timing resolution for the trench sensor is over three times better than that for the hexagonal pixel as the weighting field is far more uniform within its active region.

Declaration of competing interest

The authors declare that they have no known competing financial interests or personal relationships that could have appeared to influence the work reported in this paper.

Acknowledgements

Support is acknowledged from the STFC, UK, INFN Cagliari, Italy, the Turing Scheme Manchester, Italy and the PISA Meeting, Italy.

References

[1] M. Aresti, et al., A sub-picosecond precision laser-based test station for the measurement of silicon detector timing performances, IEEE Nuclear ScienceSymposium and Medical Imaging Conference, 2020.
[2] S. Parker, C. Kenney, J. Segal, 3D — A proposed new architecture for solidstate radiation detectors, Nucl. Instrum. Methods Phys. Res. A 395 (3) (1997) 328–343.
[3] A. Lai, Results on sensors and electronics developments for future vertex detectors, HSTD12, Hiroshima, 2019.
[4] C. Da Via, G. Dalla-Betta, S. Parker, Radiation sensors with three-dimensional electrodes, 2019.
[5] L. Anderlini, et al., Intrinsic time resolution of 3D-trench silicon pixels for charged particle detection, J. Instrum. (2020).
[6] A. Lampis, Sub-pixel characterization of innovative 3D trench-design silicon pixel sensors using ultra-fast laser-based testing equipment, Trento Workshop on Advanced Silicon Radiation Detectors, 2021.
[7] A. Lai, 3d Silicon Sensors with Timing, Manchester, 2017.
[8] A. Lai, Reading 4D-pixels at 20 ps in cmos 28-nm technology, International Workshop on Radiation Imaging Detectors, Riva del Garda, Italy, 2022.